Polymer Testing 82 (2020) 106315

Contents lists available at ScienceDirect

Polymer Testing

journal homepage: http://www.elsevier.com/locate/polytest

Preparation and characterization novel dioctyl terephthalate blended polyvinyl alcohol-composite films incorporated with the graphene oxide and silver nanoparticles

Özge Bildi Ceran [a], Barış Şimşek [a,*], Osman Nuri Şara [b]

[a] Department of Chemical Engineering, Faculty of Engineering, Çankırı Karatekin University, 18120, Çankırı, Turkey
[b] Department of Chemical Engineering, Faculty of Engineering and Natural Sciences, Bursa Technical University, Bursa, 16310, Turkey

ARTICLE INFO

Keywords:
Graphene oxide
Polyvinyl alcohol-dioctyl terephthalate composite films
Hydrophilic
Silver nanoparticles
TOPSIS based taguchi method
Waste PET

ABSTRACT

Dioctyl terephthalate is of great interest as a replacement for the phthalate plasticizers such as dioctyl phthalate and diisononyl phthalate due to its orthophthalate-free and non-carcinogenic properties. This study focused on the production, characterization and optimization of the quality characteristics of its film properties, such as the mechanical, hydrophilic and thermal properties of dioctyl terephthalate-blended polyvinyl alcohol composites modified with graphene oxide and silver nanoparticles using TOPSIS (Technique for Order Preference by Similarity to an Ideal Solution) based Taguchi Method. Dioctyl terephthalate has brought remarkable features, such as high elastic modulus, and hydrophilic and thermal stability to the polyvinyl alcohol matrix. The optimum Dioctyl terephthalate -blended polyvinyl alcohol films have a 2.26 times lower contact angle and a 13.41 times higher elastic modulus than the reference polyvinyl alcohol film. Dioctyl terephthalate should be preferentially used to manufacture more durable and hydrophilic composite films such as fibers, disposable underpad or industrial swab, instead of toxic phthalate plasticizers.

1. Introduction

Polyethylene terephthalate (PET) has a broad application due to its properties, such as its low cost, light weight, durability and flexibility [1]. Increasing PET production is raising such a question of its disposal as waste [2]. In the European Union and the UK, it has been stated that plastic wastes constitute 10–13% of municipal solid waste, and 7 wt% (1.7 million tons) of these solid wastes originate from PET [3]. Some solutions such as disposal in landfill [4], through pyrolysis or chemical recovery, have been proposed for recycling PET wastes [5,6]. However, landfills are far from being a complete solution to its disposal because they occupy too much storage area and it is costly [5,7]. The pyrolysis disposal process of PET particularly involves high energy costs, and carbon and toxic gas emissions [8,9]. Chemical recycling of waste PET, on one hand, create benefit from the recovery of certain low molecules, but, on the other hand, it will pave the way for the production of valuable chemicals [10]. The products obtained from its chemical recycling might be monomeric compounds, such as dimethyl terephthalate, bis(2-hydroxyethyl) terephthalate, bis(2-ethylhexyl) terephthalate or terephthalic acid, which can be used for the production of PET or other synthetic chemicals [11]. The chemicals that can be obtained through the chemical recovery of PET are more preferred than disposal by processes such as pyrolysis, which causes environmental pollution problems from the material [12].

Bis (2-ethylhexyl) terephthalate – also known as dioctyl terephthalate (DOTP) – is an important plasticizer because it is less volatile, has a lower viscosity, and has a higher electrical resistance than other plasticizers. DOTP also does not contain orthophthalate, and it is an important alternative to the carcinogenic plasticizers that do [13,14]. DOTP is used to produce polymer matrices in copolymers, dyes, unsaturated polyesters, polyisocyanurate foams, textile softeners, polyurethane coatings, cementitious materials [8,11,15–19] and also medical devices [20]. Producers have been increasing their annual DOTP production amounts to answer customer demands in recent years [21,22]. For example, in 2017, the BASF group sold 12% more DOTP compared to the same period in the previous year and, based on these sales figures, BASF has decided to increase its DOTP production capacity [23].

Researchers are making serious efforts to obtain a more efficient chemical recycling process. For example, Chen et al. [24] used isooctyl

* Corresponding author.
E-mail address: barissimsek@karatekin.edu.tr (B. Şimşek).

https://doi.org/10.1016/j.polymertesting.2019.106315
Received 20 November 2019; Received in revised form 23 December 2019; Accepted 25 December 2019
Available online 2 January 2020

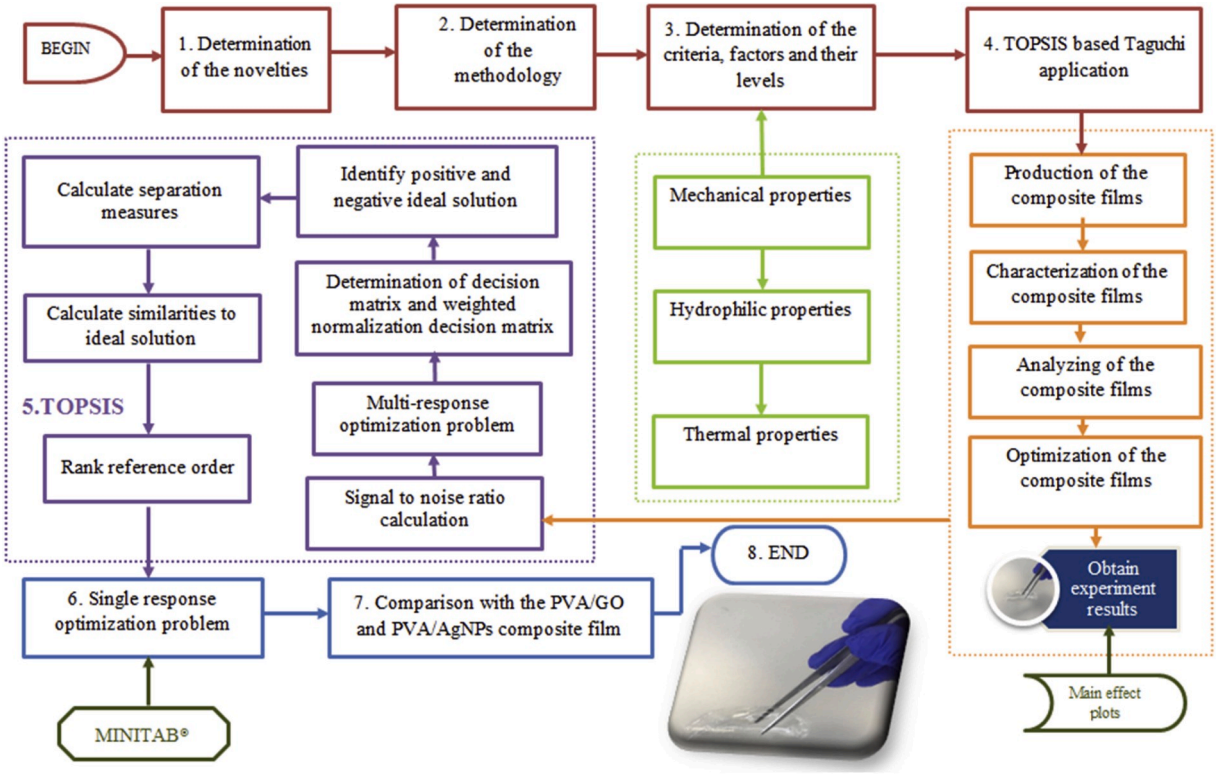

Fig. 1. Proposed framework.

alcohol, with ionic liquid as a solvent, to produce DOTP from PET wastes. They improved the alcoholysis process cost and production yield. Ding et al. [10] studied the alcoholysis kinetics of PET in sub- and supercritical isooctyl alcohol to produce DOTP. They obtained a high yield of DOTP by controlling the supercritical isooctyl alcohol. Torpanyacharn et al. [25] developed methacrylated precursors for the production of bis(2-hydroxyethyl) terephthalate from PET. Ho et al. [26] enhanced the catalytic glycolysis conditions for the chemical recycling of glycol-modified PET. They improved the reaction rate by three times, under optimum conditions, relative to glycolysis produced with conventional zinc acetate. Zhou et al. [27] synthesized DOTP from the alcoholysis of PET, using 2-ethyl-1-hexanol as the solvent, and choline chloride-based deep eutectic solvents as the catalysts, due to their cheapness and low toxicity. They improved the conversion amount of PET and determined the optimum parameters. Several investigations have been conducted by researchers to develop application areas for DOTP, and to determine the properties of DOTP-doped products due to the above-mentioned features of such materials. Şimşek et al. [28] added DOTP to concrete, reporting that the electrical resistance of the concrete increased with increased amounts of DOTP. They also found that DOTP could be used in building materials due to its high corrosion resistance [5]. Viante et al. [8] developed a new composite, using the bis (2-hydroxyethyl) terephthalate monomer obtained from the catalyzed glycolysis of PET, to prepare magnetic microspheres, thus presenting a new field for the evaluation of PET wastes. The results of previous studies have proved that the beneficial effects of DOTP on other materials will gradually increase.

The ability to design composite films is of great interest [29] because of the increased demand for new and emerging flexible, packaging and medical technologies [30]. Composite films are very attractive [31] for photovoltaics [32], hydrophobic [33] or hydrophilic transparent surface [34], electrodes [35], transistors [36], solar cells [37], lithium ion batteries [38], energy storage [39], textiles products [40], packaging technology [41] and biosensor applications [42] and the production of the diapers or bandages for medical sectors [20]. DOTP can be a suitable material for film production due to its above-mentioned properties.

Polyvinyl alcohol (PVA) is one of the preferred film-forming materials because it is non-toxic and non-carcinogenic, and has high thermal stability, high optical permeability, high flexibility and chemical resistance [43–46]. Nanomaterials have been used as filling material in recent years due to their superior mechanical properties [47–49]. Moreover, graphene oxide (GO) [50–55] and silver nanoparticles (AgNPs) [56–59] are widely used to provide high tensile strength, elongation at break, thermal stability and electrical conductivity, and they also have antibacterial properties. These materials were selected for this study in order to produce a film matrix with DOTP.

The novelties of this study are i) production and characterization of novel PVA/DOTP and PVA/DOTP-composite films incorporated with GO and AgNPs, ii) investigation of the mechanical, hydrophilic, morphological and thermal properties of DOTP-doped composite films by statistical methods, iii) disposal of DOTP obtained by the chemical recycling of PET, which causes serious environmental problems, in composite film production and the revelation of industrial applications for DOTP-doped PVA nanocomposites, using a multidimensional analysis of product properties.

2. Materials and method

2.1. Materials

Polyvinyl alcohol (Mw~125,000 and 8.0–98.8 mol% hydrolysis), silver nitrate (≥99.5%), starch (from potato), and hydrogen peroxide (34.5–36.5%) was supplied from Sigma Aldrich. Graphite (<50 μm), potassium permanganate (extra pure), D (+) - Glucose (anhydrous for biochemistry), sodium hydroxide pellets used for pH adjustments (NaOH,> 99%), sulfuric acid (95–97%), ortho phosphoric acid (85%) was obtained from Merck Millipore. An improved Hummers' method was preferred as a green solution in order to synthesis GO [60,61]. A green method [62], using glucose as a reducing agent and starch solution from potatoes as a capping agent, was selected to synthesize AgNPs

Table 1
Experimental design and mixture details.

Sam	Exp. No.	Factors have been determined according to preliminary test results (g)						Thickness (μm)	C/O atomic ratio
		PVA amount (g)	DOTP (g[a] or %[b])	Stirring time (min)	Sample amount (ml)	GO amount	Glucose to AgNO3 mole ratios		
Ref.	PVA1	1.2	N/A	60	15	N/A	N/A	98.4	2.79
DP	DP1	1.0	0.027	30	15	N/A	N/A	58.8	2.02
	DP2	1.0	0.075	60	20	N/A	N/A	67.2	1.91
	DP3	1.0	0.122	90	25	N/A	N/A	199.4	3.55
	DP4	1.2	0.027	60	25	N/A	N/A	76.2	1.96
	DP5	1.2	0.075	90	15	N/A	N/A	86.8	2.12
	DP6	1.2	0.122	30	20	N/A	N/A	226.0	3.89
	DP7	1.4	0.027	90	20	N/A	N/A	153.6	1.89
	DP8	1.4	0.075	30	25	N/A	N/A	189.4	2.04
	DP9	1.4	0.122	60	15	N/A	N/A	161.4	1.88
Ref.	PVA2	1.2	N/A	60	15	N/A	N/A	121.0	2.79
DPG	DPG1	1.2	2.25	30	15	0.012	N/A	63.0	1.90
	DPG2	1.2	6.25	60	20	0.012	N/A	79.2	1.99
	DPG3	1.2	10.15	90	25	0.012	N/A	145.4	4.28
	DPG4	1.2	2.25	60	25	0.018	N/A	113.0	1.96
	DPG5	1.2	6.25	90	15	0.018	N/A	67.0	1.91
	DPG6	1.2	10.15	30	20	0.018	N/A	107.6	2.16
	DPG7	1.2	2.25	90	20	0.024	N/A	78.0	1.93
	DPG8	1.2	6.25	30	25	0.024	N/A	94.2	2.10
	DPG9	1.2	10.15	60	15	0.024	N/A	70.4	2.40
Ref.	PVA2	1.2	N/A	60	15	N/A	N/A	113.0	2.79
DPA	DPA1	1.2	2.25	30	15	N/A	5	88.2	1.85
	DPA2	1.2	6.25	60	20	N/A	5	88.4	1.90
	DPA3	1.2	10.15	90	25	N/A	5	160.0	4.25
	DPA4	1.2	2.25	60	25	N/A	10	174.8	1.82
	DPA5	1.2	6.25	90	15	N/A	10	89.2	2.10
	DPA6	1.2	10.15	30	20	N/A	10	194.2	3.30
	DPA7	1.2	2.25	90	20	N/A	15	76.6	2.05
	DPA8	1.2	6.25	30	25	N/A	15	154.8	2.69
	DPA9	1.2	10.15	60	15	N/A	15	86.4	4.26

[a] for DP.
[b] for DPG and DPA.

[63]. DOTP was procured from the Meltem Kimya Company [28]. Detail information about synthesis and characterization of GO, AgNPs and DOTP can be seen in the supplementary material appendix A.

2.2. Method

The Taguchi method is an experimental design method based on the principle of minimizing the duration of the experiment and reducing the cost of the test using orthogonal arrays [64,65]. This method is widely used to improve the product quality, with the decreasing process variance and accelerate the product development activities [66]. The optimization design based on the Taguchi method aims to determine an optimum quality factor which has a great impact on the quality characteristics of the product. In Taguchi method, Signal/Noise (S/N) ratios are used to evaluate the product quality. These S/N ratios are classified in three ways as the lower is better, the nominal is better and the higher is better, depending on their characteristics [60,61,64,65].

However, it is not possible to use Taguchi Method for simultaneous optimization of multiple quality criteria. In order to make it possible to do a multiple-response optimization using Taguchi Method, in this study, Taguchi Method is combined with TOPSIS (Technique for Order Preference by Similarity to an Ideal Solution) Method. The advantage of the TOPSIS-based Taguchi method is that it involves simpler calculations compared to the other complex multi-response optimization methods. In Taguchi method, "the highest is the best" signal to noise ratios (S/N) ratios and "the lowest is the best" S/N ratios are calculated for each criterion. Responses converted to S/N ratios are referred to the "decision matrix". The weighted decision matrix is calculated by weighting the responses. Details of the method are given in Şimşek et al. [60,61,64,65].

The proposed methodology for the production and characterization of the novel PVA/DOTP and PVA/DOTP Composite Films Incorporated with the GO and AgNPs are shown in Fig. 1.

3. Experimental design

The hardness and elastic modulus of the PVA/DOTP composite films incorporated with GO and AgNPs were selected as the two quality criteria (responses) to indicate the mechanical properties. A Berkovich-type indenter, with a 0.1–400 mN nanoindentation load range, was used to measure these features [67–70]. In order to avoid the effect of the substrate on a film's mechanical properties, the maximum depth of indentation was fixed at 200 nm, which was less than one-tenth to one-seventh of the total thickness [69]. The load and unload times were both 10 s, and the displacement speed of the indenter was 20 nm/s. The same test was repeated six times on each sample. The hardness and elastic modulus of the composite films should be at a maximum for the production of durable and flexible thin films. The third quality criterion (response) selected was the contact angle, which indicates the hydrophilic properties composite film. The quality criteria and determined weights for the PVA/DOTP composite films incorporated with GO and AgNPs are summarized in supplementary material appendix B, Table B1. Four three-level factors, having major effects on the properties of PVA/DOTP composite films incorporated with GO and AgNPs were selected to build an experimental design matrix. The definitions, symbols and levels of the factors are shown in supplementary materialappendix B, Table B2.

An Attension theta-type tensiometer was used to measure the contact

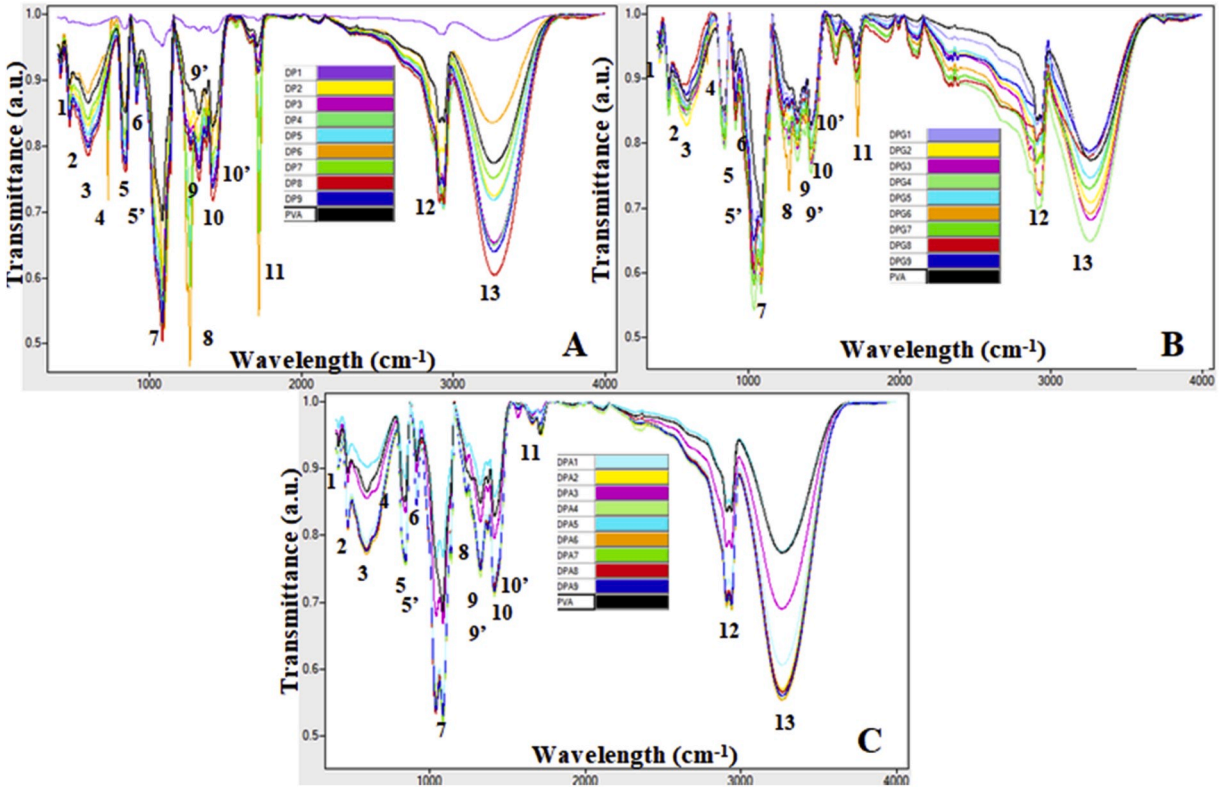

Fig. 2. FTIR spectra a) DP b) DPG and c) DPA.

angles of the composite film samples. The contact angle of PVA/DOTP composite films must be minimized to produce thin films with hydrophilic surfaces that can be used as, for example, solar cells, periscopes and lenses, and other biological and environmental applications [71,72]. The other quality criteria selected were specific heat capacity (thermal energy storage capability) and weight loss (thermal

Table 2
FTIR spectrum table for composite films.

Designated number	Functional group/vibration	Region	Intensity	Related material	Ref.
1,2 and 3	$C-H$ *bending*	@415-600 cm^{-1}	Very strong	DOTP/PVA/GO	[75]
4	$C-H$ *bending benzene deritative*	@728 cm^{-1}	Very strong	DOTP	[75]
5	$C=C$ *bending alkene*	@829 cm^{-1}	Too weak	PVA	[76]
5′	$C-H$ *bending benzene* $1,4-$ *disubstituted*	@850 cm^{-1}	Strong	DOTP	[75]
6	$(C-O)$ *stretching vinyl ether*	@1018 cm^{-1}	Strong	DOTP	[24]
	$(C-OH)$*hydroxyl*	@1030 cm^{-1}	Weak	GO	[77]
	$(C-N)$ *stretching amines*	@1043 cm^{-1}	Weak	AG	[51]
7	$(C-O)$*stretching secondary alcohol*	@1100 cm^{-1}	Strong	PVA	[51]
	$(C-O-C)$ *stretch*	@1100 cm^{-1}	Very Strong	DOTP	[24]
8	$(C-O)$*stretching aromatic ester*	@1247 cm^{-1} @1264 cm^{-1}	Very Strong	DOTP	[77]
9	$(C-O)$*stretching alcohols*	@1327 cm^{-1}	Strong	PVA	[51]
9′	(CH_3)*bends*	@1380 cm^{-1}	Very Strong	DOTP	[24]
	$(C=C)$*aromatic*	@1390 cm^{-1}	Strong	GO	[78]
10	(CH_2)*bends*	@1407 cm^{-1}	Strong	DOTP	[10]
	(OH)*bending alcohols, carboxylic acid*	@1417 cm^{-1}	Medium	PVA	[76]
10′	(CH_2)*bends*	@1462 cm^{-1}	Strong	DOTP	[79]
11	$(C=O)$ *carboxylic acid, ketone*	@1710 cm^{-1}	Too weak	PVA	[76]
	$(C=O)$ *carboxylic acid*	@1710 cm^{-1}	Medium	GO	[80]
	$(C=O)$ *carboxylic acid, ketone*	@1719 cm^{-1}	Strong	DOTP	[10]
	$(C-C)$ *stretching non conjugated*	@1743 cm^{-1}	Weak	AG	[81]
12	$C-H$ *stretching*	@2910 cm^{-1}	Medium	PVA	[76]
		@2860 cm^{-1}	Medium	DOTP	[10]
		@2890 cm^{-1}	Weak	GO	[82]
		@2921 cm^{-1}	Weak	AG	[81]
13	(OH) *alcohols and phenol*	@3262 cm^{-1}	Strong	PVA	[76]
		@3290 cm^{-1}	Strong	GO	[80]
		@3421 cm^{-1}	Strong	AG	[81]

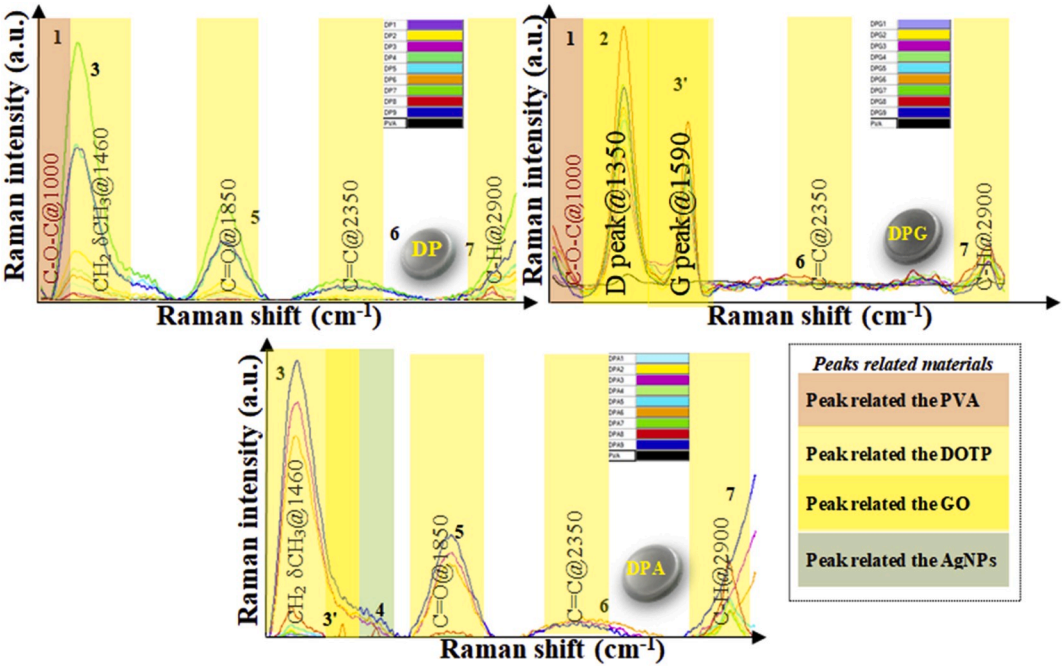

Fig. 3. Raman spectra a) DP b) DPG and c) DPA.

stability). The specific heat capacity of composite films should be maximized to improve their energy storage capabilities [73] while the weight loss of composite films should be minimized to enhance their thermo stability properties [74]. The specific heat capacity and weight loss values of the composite films were determined using TA Instruments Differential Scanning Calorimeter (DSC) Q200 and Thermal Gravimetric Analysis (TGA) Q500 devices. Solution casting method was used to produce DOTP/PVA (DP), DOTP/PVA/GO (DPG) and DOTP/PVA/AgNPs (DPA) composite films. Detail information about synthesis process and quality criteria of produced composite films can be seen in the supplementary material appendix B.

L_9 (3^4) orthogonal array was selected for carrying out the experiments. Experimental design including the details of the mixture design is given in Table 1. The thickness and carbon to oxygen atomic ratios (C/O) of the PVA/DOTP composite films incorporated with the GO and AgNPs can be seen in Table 1.

The results of the conducted experiments for PVA/DOTP composite films incorporated with the GO and AgNPs (data set) are also given in supplementary material Appendix C, Table C1.

4. Results and discussion

4.1. Characterization of PVA-DOTP composite films incorporated with nanomaterials

FTIR analysis: Fourier Transform Infrared spectroscopy (FTIR) was used to characterize the synthesized PVA-DOTP composite films incorporated with GO and AgNPs. The FTIR spectra of the PVA control film and PVA-DOTP films were recorded to compare the chemical changes in the film matrices of the DP composite films; the spectra are shown in Fig. 2A. High-intensity peaks were centered at 415-600 cm^{-1}, 728 cm^{-1}, 829 cm^{-1} and 850 cm^{-1} (symbolized as 1–5), which are related to a C–H-bending benzene derivative, C–H-bending benzene 1, 4-disubstituted and C–O vinyl ether stretch, referring to the DOTP structure. As expected, peak intensity at 1020 cm^{-1} (symbolized as 6) was decreased in the composite films incorporating GO and Ag^0. Strong peaks at 1100 cm^{-1}, 1247 cm^{-1} and 1327 cm^{-1} (symbolized as 7, 8 and 9) are associated with C–O stretching alcohol or aromatic ester, which appeared strongly in the PVA, DOTP and GO spectra, and were clearly seen in all the composite films (Fig. 2B and C). CH_3 methyl stretching and C═C aromatic stretching (symbolized as 9′) were robustly present in the spectra of the DOTP and GO (Table 2). For this reason, this was a very strong peak in the DP composite films and a strong peak in the DPG composite films; while it was almost absent from the DPA composites. The peaks at 1380 cm^{-1} and 1410 cm^{-1} (symbolized as 9' and 10), attributed to methylene (–CH_2–) bending, and the hydroxyl group were clearly seen in all the composite films, as expected. As the amount of DOTP increased in the PVA matrix, and mixing time such as DP8 and DP9, the intensity of the peak at 1720 cm^{-1}, related to C═O stretching (symbolized as 11), was considerably reduced (Fig. 2A). Apparent absorption bands at 2900 cm^{-1} and 3260 cm^{-1} are related to C–H stretching and hydroxyl groups belonging to DOTP, PVA, GO and Ag^0 were seen in the all composite films (symbolized as 12 and 13). Moreover, no new peaks were observed in the spectra of the composite films, proving that no other chemical interactions occurred between the materials.

Raman analysis: The Raman shift positions of three weak spectral peaks at 1000 cm^{-1} (symbolized as 1), observed in all composite films, belong to the PVA (Fig. 3A–C) [83]. A strong band at 1350 cm^{-1} was clearly seen in the DPG composite films, as expected (symbolized as 2; Fig. 3B). Owing to the in-phase CH_3 methyl and CH_2 methylenes stretching of the DP composite films, a strong Raman peak appeared at around 1460 cm^{-1} (symbolized as 3). This peak also appeared at around 1460 cm^{-1} in the DPA composite films (Fig. 3A). The peak at around 1460 cm^{-1} seems to have shifted to 1590 cm^{-1} in the films containing GO, or perhaps the GO peak at 1590 cm^{-1} (peak G) prevented this peak from appearing (symbolized as 3'; Fig. 3B). The weak band in the light green areas indicates C═C vibration in the DPA composite films, resulting from the AgNPs (symbolized as 4; Fig. 3C). With the amount of DOTP in the PVA matrix and the mixing time at medium values (e.g. DP8 and DP9), the intensity of the peak at 1850 cm^{-1} related to C═O stretching (symbolized as 5) was reduced considerably (Fig. 3A). This peak was almost completely lost in the DPG composite films (Fig. 3B). The basic chemical structure of the DOTP is the benzene ring, which contains a C═C bond at 2350 cm^{-1} (symbolized as 6), as seen in the Raman spectra of all the composite films. The intensity of the peak at 2350 cm^{-1} was decreased substantially in the DPG composite films (Fig. 3B), with the increase in C–O and C–H stretching as a result of the

Table 3
Raman spectrum table for composite films.

Designated number	Functional group/vibration	Region	Intensity	Related material	Ref.
1	$\vartheta(C-O-C)asym$	@1000 cm^{-1}	Too weak	PVA	[84]
			Medium	DOTP	This study
2	$\vartheta(C-C)alicyclic,\ aliphatic\ chain$	@1320 cm^{-1}	Too weak	PVA	[84]
	D peak	@1350 cm^{-1}	Strong	GO	[80]
3	$\vartheta(C-C)aromatic\ ring\ chain$	@1460 cm^{-1}	Strong	AG	[77]
	$\delta(CH_2)\ and\ \delta(CH_3)\ asym$		Strong	DOTP	This study
3′	$\vartheta(C-C)aromatic\ ring\ chain$	@1590 cm^{-1}	Strong	AG	[85]
	G peak		Strong	GO	[86]
4	$\vartheta(C=C)$	@1660 cm^{-1}	Weak	AG	[77]
5	$\vartheta(C=O)$	@1850 cm^{-1}	Medium	DOTP	This study
6	$\vartheta(C=C)$	@2350 cm^{-1}	Weak	DOTP	This study
7	$\vartheta(C-H)$	@2900 cm^{-1}	Weak	PVA	[84]
	D + D′ peak		Too weak	GO	[87]
	$\delta(CH_3)\ asym$		Medium	DOTP	This study

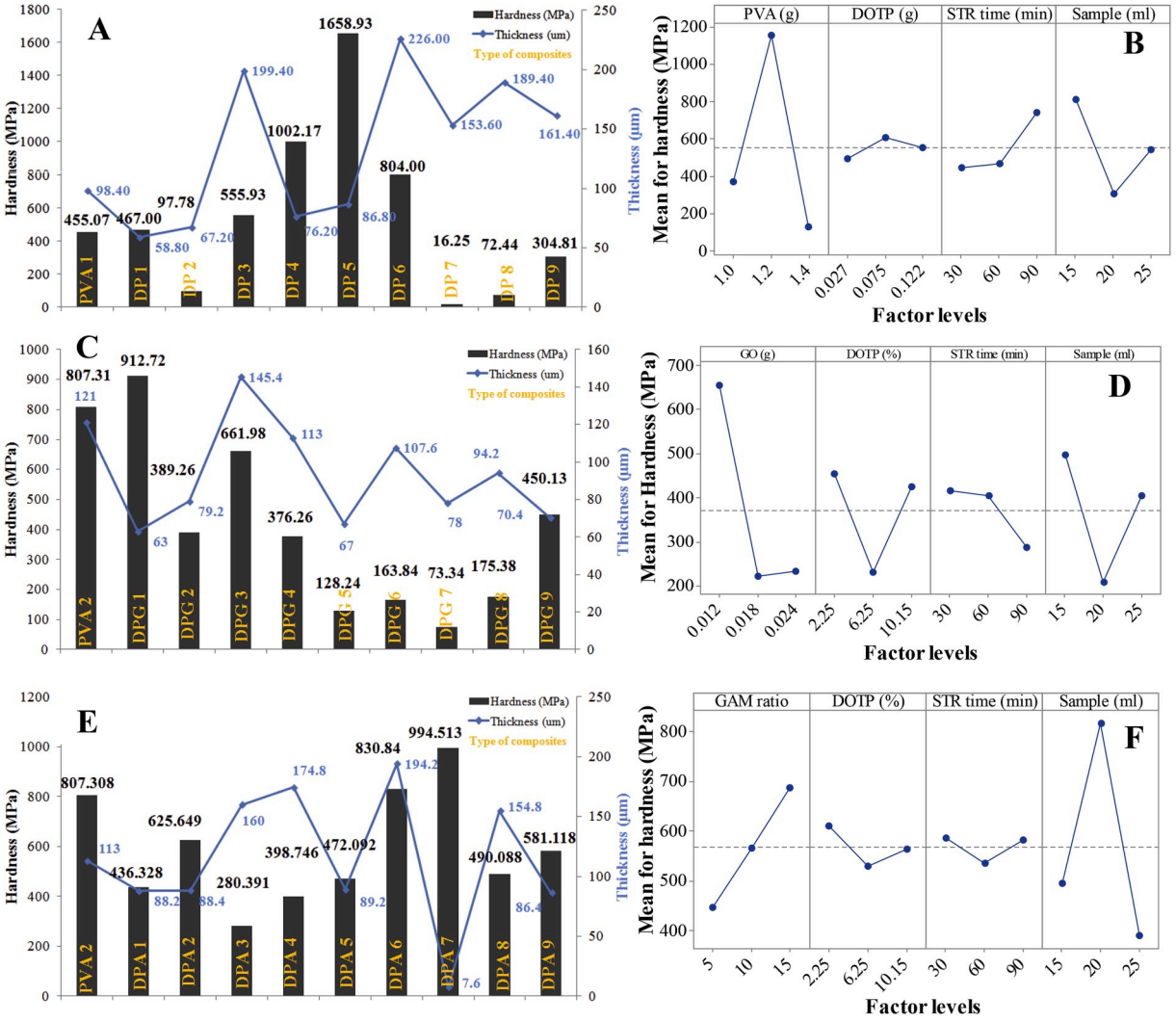

Fig. 4. Hardness and thickness of composite films as a function of factors: a) DP b) DPG and c) DPA, main effect graphics for composite films: d) DP e) DPG and f) DPA.

PVA/GO and DO/DOTP interactions. Also, a relatively weak peak occurred in the 2850 cm^{-1}–2930 cm^{-1} (symbolized as 7) orange region due to the in-plane rocking of CH_3 groups attached to the benzene chain, and C–H vibration (Fig. 3A–C). These results demonstrate that Raman spectroscopy is a very useful tool for characterizing PVA/DOTP composite films incorporated with nanomaterials such as GO and AgNPs. Table 3 shows the Raman spectra for the materials used to manufacture the composite films.

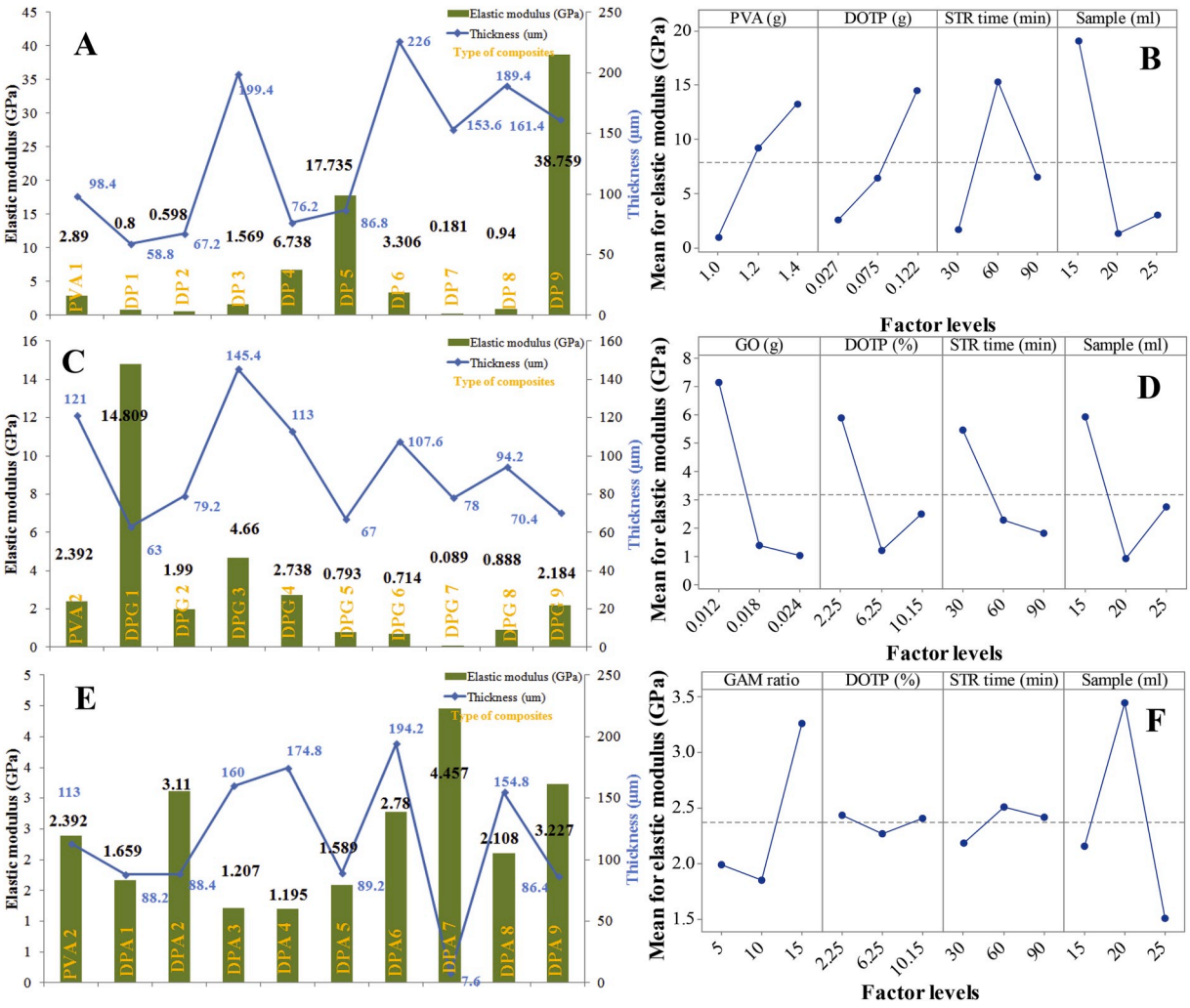

Fig. 5. Elastic modulus of composite films as a function of factors: a) DP b) DPG and c) DPA, main effect graphics for composite films: d) DP e) DPG and f) DPA.

4.2. Mechanical properties

Fig. 4A–C shows the variation in hardness with the change in factor level and film thickness. The hardness of the DP composite films reaches the highest value using a moderate PVA and DOTP level, with an 86.80 μm average thickness (DP5; Fig. 4A). Whilst the hardness of the DP composite films increased with increasing PVA and DOTP, it decreased dramatically when the usage of DOTP and PVA exceeded 0.075 g and 1.2 g, respectively. Above this point, the amount of PVA and DOTP was increased by decreasing the mixing time. Therefore, it can be said that adequate mixing was not achieved, and the sample had lost its homogeneity. Moreover, the thicknesses of the DP composite films contained high amounts of PVA and DOTP were almost twice as much as the DP films with moderate amounts of PVA and DOTP. It can be seen from the main effects of the analyzed responses (Fig. 4B), plotted using experimental design analysis, that the hardness of the DP composite films increased as the mixing time increased. The main effect of the DP composite films confirmed that film hardness increased with moderate DOTP and PVA usage, and decreased with high PVA and DOTP (Fig. 4B). The hardness of the DPG composite films decreased dramatically with the increasing GO amount significantly (Fig. 4C and D and). Even though the amount of nanomaterial used in thin films can be increased using the given methods, the generally accepted opinion is that nanoparticles tend to agglomerate in the presence of aqueous media due to the strong van der Waals forces [88]. Furthermore, the interaction effect between molecules, such as H bonds, which can be seen in Fig. 4B, and van der Waals forces has caused GO flake dispersion in the PVA matrix to become difficult. Increasing the mixing time did not prevent the agglomeration in the DPG composite films (Fig. 4D). The hardness of the DPA composite films reached its peak with the use of moderate PVA and low DOTP amounts, and with a 7.6 μm average thickness (DPA7; Fig. 4E). It is noteworthy that a high hardness value was obtained at this thickness. It was observed that, as the glucose to $AgNO_3$ ratio increased (in other words, the particle size of the AgNPs decreased), the hardness of the DPA films increased. This is because nanoparticles with a smaller particle size form a more homogeneous and non-aggregating PVA-based mixture matrix (Fig. 4F). A more successful hardness performance was achieved with low amounts of DOTP and 2.25% (w/w) PVA (Fig. 4F).

One of the most striking results was the elastic modulus of the DP composite films. The DP5 composite film, with an 86.8 μm thickness, and the DP9 composite film, with a 161.4 μm thickness, had 6.14 and 13.41 times higher elastic modulus, respectively, than the reference PVA film, with a 98.4 μm thickness (Fig. 5A). The elastic modulus of the DP composite films increased with increasing amounts of PVA and DOTP (Fig. 5B). Low stirring times and amounts of sample produced composites with higher elastic modulus (Fig. 5B). The elastic modulus of the DPG1 composite films, with 1% GO (w/w) and 2.25% DOTP (w/w for PVA film), with a 63 μm thickness, achieved a 6.19 times higher elastic modulus than the reference PVA film, with a 121 μm thickness (Fig. 5C). Above this point, it decreased dramatically (Fig. 5D) due to agglomeration, similarly to the hardness results. Increasing the mixing time did not affect in the DPG composite films' elastic modulus values (Fig. 5D).

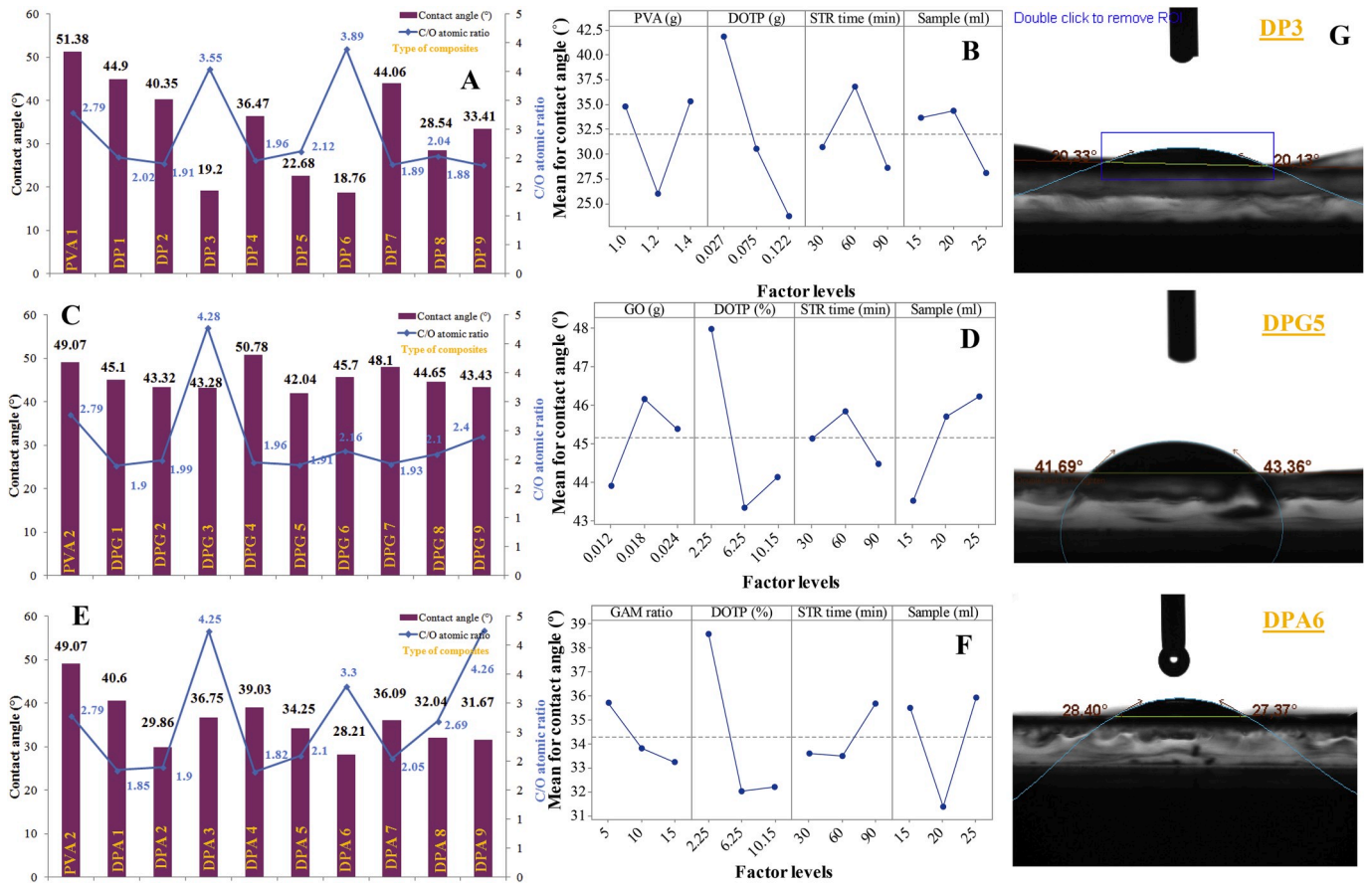

Fig. 6. Contact angle of composite films as a function of factors: a) DP b) DPG and c) DPA, main effect graphics for composite films: d) DP e) DPG and f) DPA, g) photographs of water droplet that placed on the composite films: DP3, DG5 and DPA6.

Furthermore, DOTP enhanced the elastic modulus of the composite film when used only in a PVA matrix. However, when DOTP was used with GO in a PVA matrix, it decreased the elastic modulus of the composite film due to the agglomeration problem of the nanomaterial. The DP composite film modified with AgNPs with the highest elastic modulus was DPA7, with a 7.6 μm thickness (Fig. 5E). It is also noteworthy that a high elastic modulus was obtained at this thickness, similarly to the hardness test results. The main result that can be deduced from the effect plot is that, as the glucose: $AgNO_3$ ratio increases (in other words the particle size of the AgNPs decreases), the elastic modulus values of the composite films increases (Fig. 5F) due to low agglomeration. It is evident that nanomaterials used in large amounts overshadow the positive effects of DOTP on hardness and elasticity. The mechanical test results showed that a long mixing time provided more successful homogenization of the composite films. Moreover, the disadvantage of the films synthesized at this point is the loss of homogeneity due to the addition of nanomaterials. However; this problem did not occur with small size silver nanoparticles, but graphene oxide which tended to agglomerate caused the homogeneity problem. The capping agent (soluble starch from potato) used in silver nanoparticle synthesis prevented agglomeration and thus a more homogeneous DPA film was obtained. Homogeneity problem in DPG composite films can be overcome by the use of surfactants during the addition of graphene oxide into the PVA matrix.

4.3. Hydrophilic properties

A 3 μl of distilled water droplet was deposited onto the surface of the composite films. Measurements were taken as the droplet receded, including the contact angle within 5 s [89]. The measured contact angles are presented as a function of the variation in factor level of the composite films. The average contact angle values of six repetitions of PVA-DOPT composite films incorporating nanomaterials were calculated.

Composite films DP6, with an 226 μm thickness, DP3, with a 199.4 μm thickness, and DP5, with a 86.8 μm thickness, achieved a 2.73, 2.67 and 2.27 times lower contact angle, respectively, than the reference PVA film, with a 98.4 μm thickness (Fig. 6A). Another result was that the contact angle of the DP composite films decreased as the carbon: oxygen atomic ratio increased (Fig. 6A and 3.55 for DP3 and 3.89 for DP6). The main effect plot of the contact angle for the DP composite films clearly shows that their contact angles decreased with increasing DOTP (Fig. 6B, D and 6F). The contact angle for DPG5 which had the lowest value decreased from 49.07° to 42.04° (Fig. 6C). DPA6, which had a high carbon: oxygen atomic ratio of 3.3, with a 194.2 μm thickness, had a 1.73 times lower contact angle than the reference PVA film, with a 98.4 μm thickness (Fig. 6E). The amount of PVA and the stirring time should be kept at moderate levels (Fig. 6B, D and 6F). The contact angles of the composite films decreased when the glucose: $AgNO_3$ ratio increased (in other words, the particle size of the AgNPs decreased; Fig. 6F). Images of the water droplets placed on the composite films, such as DP3, DG5 and DPA6, are included in Fig. 6G. At this point, the application of mixing more or less than necessary, adversely affects the contact angle property of the films. This disadvantage can be eliminated by optimization study.

4.4. Thermal properties

It is necessary to know the thermal properties of materials, such as their specific heat capacity and weight loss, in order to understand their

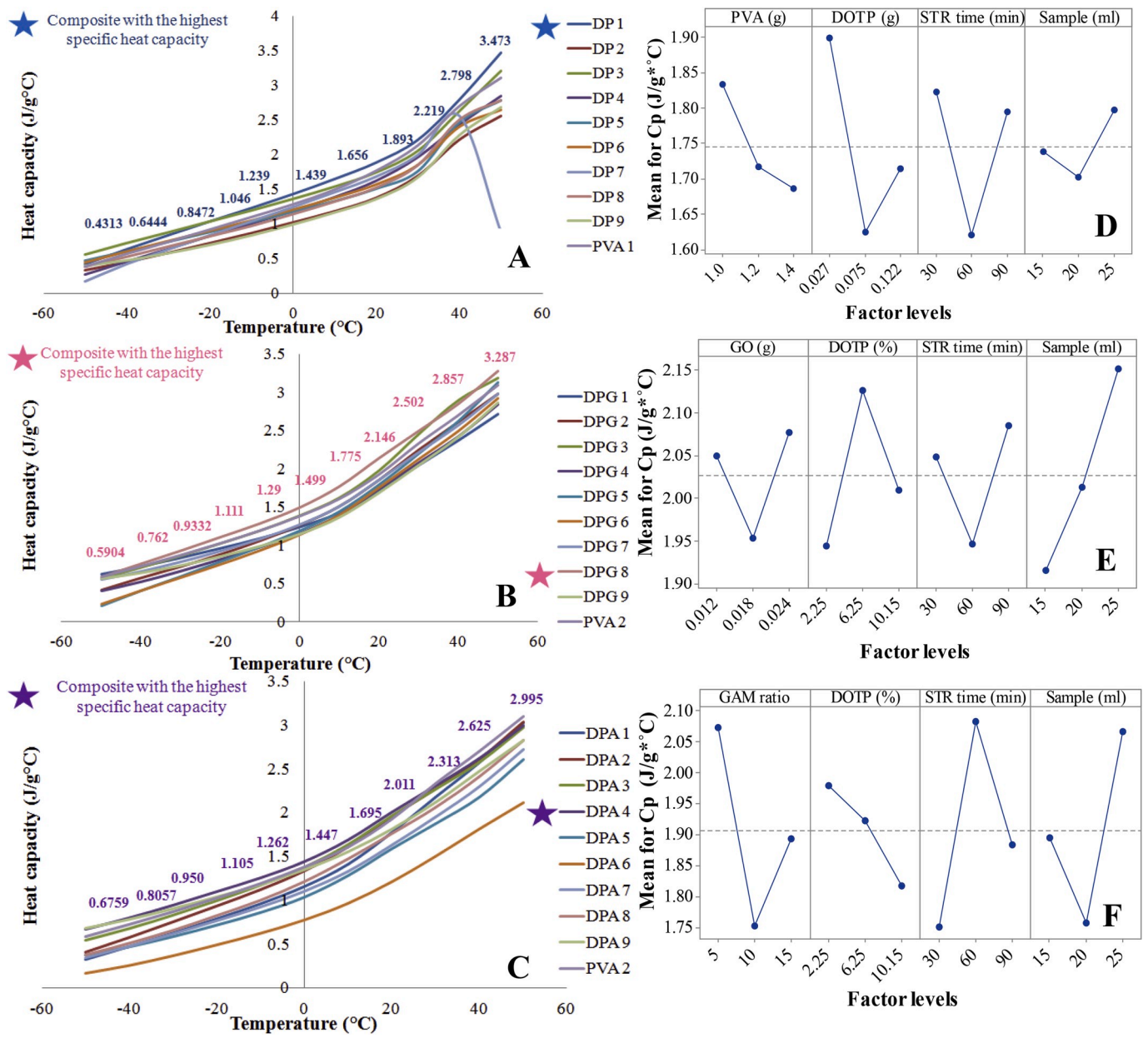

Fig. 7. Heat capacity of composite films as a function of factors: a) DP b) DPG and c) DPA, main effect graphics for composite films: d) DP e) DPG and f) DPA.

thermal behavior. Fig. 7 illustrates the specific heat profiles, at constant pressure, as a function of the factor levels of the DP composite films investigated. The specific heat values measured between −60 °C and 60 °C. The composite films with the highest specific heat capacities were determined as DP1, DPG8 and DPA4. However, the specific heat capacity values of the DP composite films incorporating GO and AgNPs remained at the same level as that of the reference PVA. Based on the main effect plots, it can be interpreted that the specific heat capacity of DP composite films decreased with increasing amounts of DOTP (Fig. 7A–F).

DOTP, with its low specific capacity based composite films has an inability to store the thermal energy. However, the fact that it causes high specific heat brings thermal stability to the films that can hold a large of thermal energy, while it has the disadvantage that the films need more energy to increase their temperature.

Thermogravimetric analysis was used to determine and investigate the thermal behavior of synthesized DP composite films upon heating under a nitrogen atmosphere. Composite film samples of 6 mg weight were submitted to a heating rate of 10 °C/min using aluminum crucibles and a range of temperature from 25 °C to 600 °C.

Fig. 8 illustrates weight loss as a function of factor level of the DP composite films. The films started to decompose around 120–200 °C. The weight loss of the films was continuous up to 200–500 °C, and maximum decomposition was reached at about 600 °C. The percentage of weight loss and the temperature at the peak degradation for all the synthesized composite films are shown in Fig. 8. A sample for calculation of the maximum weight loss and temperature at maximum weight loss can be seen in the Supplementary Material-Appendix D-Figure D1. The first stage, below 200 °C, the weight loss was associated with the loss of water [90]. The second stage, at between 200 °C and 500 °C, the weight loss was due to the decomposition of chain segments of the PVA molecules and hydrogen bonding [91]. The difference in the final residues at temperature exceeding 500 °C for the DP composites corresponds to the inorganic fraction. The DP composite film with the lowest percentage weight loss was determined as DP9, with a 161.4 μm thickness, at a maximum decomposition temperature of 510 °C

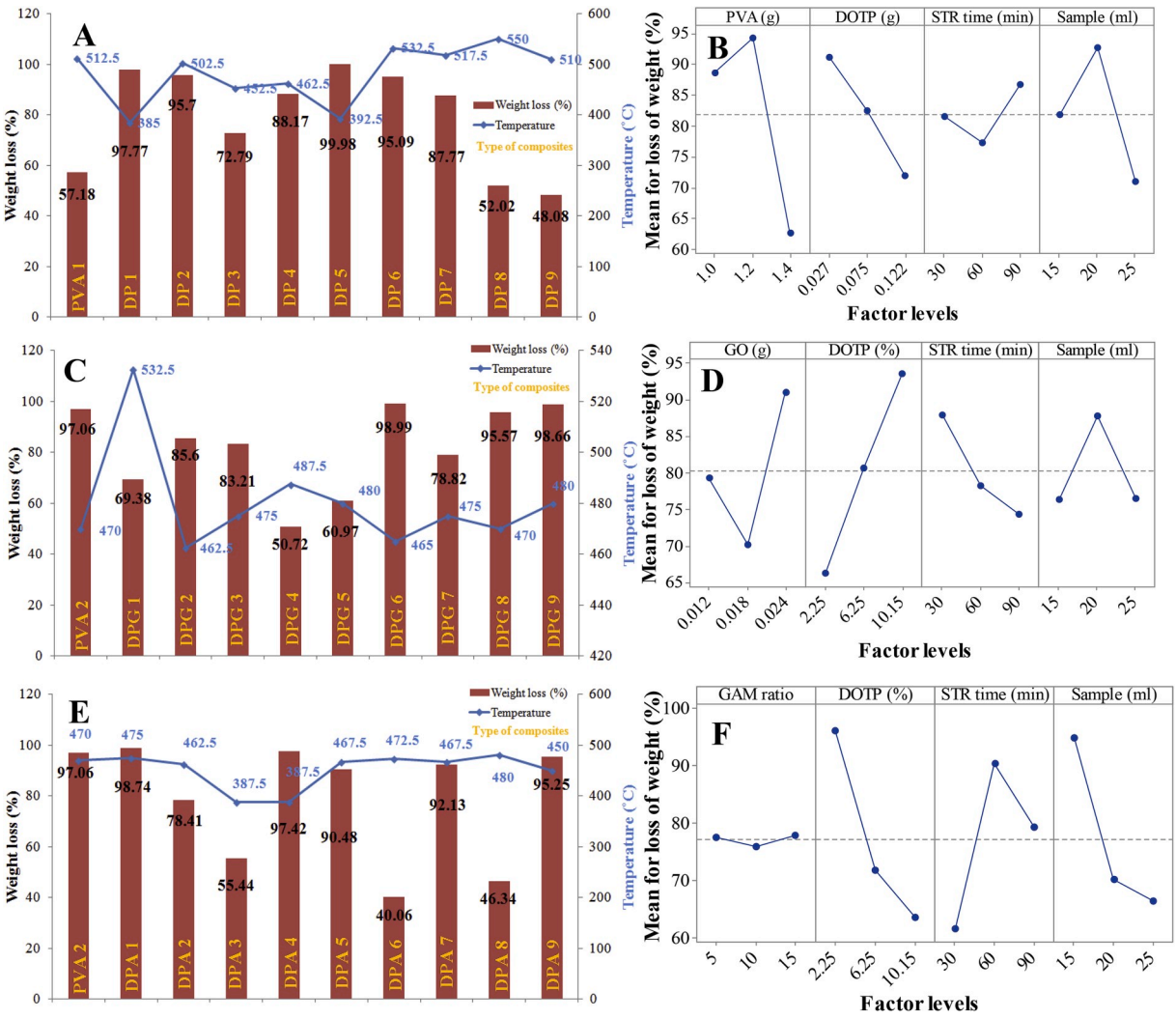

Fig. 8. wt loss of composite films as a function of factors: a) DP b) DPG and c) DPA, main effect graphics for composite films: d) DP e) DPG and f) DPA.

(Fig. 8A). The percentage weight loss of the DP composite films decreased with increasing amounts of PVA and DOTP (Fig. 8B). DPG4 had the lowest percentage weight loss, with a 113 μm thickness, at a maximum decomposition temperature of 487.5 °C (Fig. 8C). Based on the main effect plots, the interaction of the DOTP and PVA negatively affected the thermal stability of the DPG composite films (Fig. 8D). The reasons for this may be the strong hydrogen bonding between PVA and GO [91], and also interaction between the methyl groups in DOTP and the carboxylate or hydroxyl groups in GO. The highest thermal stability in all of the synthesized composite films was determined in DPA6, with a 40.06% weight loss (Fig. 8E). A weight loss between 472 °C and 600 °C did not occurred in DPA6. The weight loss in DPA was significantly reduced by the synergetic impact of the amount of DOTP (Fig. 8F). The minimum weight loss value was achieved from short stirring times (Fig. 8B and D), except in the DPA composite films (Fig. 8F).

4.5. Optimum design

The experimental design and the S/N ratios for the-lower-the-better and the-higher-the-better responses were calculated, respectively, for each response, and the results are given in Table 4 (Columns 2–6). The deviation values from the positive (Si*) and from negative ideal solutions were calculated (Table 4, Columns 7, 8). The deputy responses (Ci*) are also shown in Table 4 (final columns).

Three deputy responses, symbolized by Ci^1, Ci^2 and Ci^3, were determined for the DP composite films, considering the same weight assignment, hydrophilic composite film production and thermal stable composite film production, respectively. The same optimum design (maximum deputy Ci^4 and Ci^5) was achieved for the DPG and DPA values, even when different weights were assigned to the criteria. Normalization methods led to the optimum parameter design of DP5 and DP9 for the DP composite films, DPG9 for DPG for the DP composite films modified with the GO and DPA7 for DPA for the composite films modified with the AgNPs (Table 5). Improvement or deterioration ratios for the properties of the DP composite films with different weights were calculated, and are given in Table 5.

4.6. Comparison with the PVA/GO and PVA/AgNPs composite films

In order to analyze the effectiveness of DOTP additives, DP composite films modified with nanoparticles were compared to the widely used PVA/GO and PVA/AgNPs composite films, in terms of mechanical, hydrophilic and thermal performance. The greatest hardness, and highest contact angle and percentage weight loss values were found to be 381.17 MPa, 62.5° and 99% for 1% (w/w) GO-reinforced PVA composite. The hardness of DP9 was found to be 335.2% higher (1658.93 MPa), whilst the contact angle and weight loss of DP5 was found to be 63.71% and 51.43% lower, than the PVA/GO film. The elastic modulus were determined as 0.774 GPa and 1.087 GPa for the PVA composite with 1% (w/w) GO and AgNPs, respectively. DP5, with

Table 4
An example of TOPSIS method implementation for DP and deputy responses for DPG and DPA.

	Decision Matrix (S/N Ratios)					S_i^*	S_i^-	C_i^{*1}	C_i^{*2}	C_i^{*3}	C_i^{*4}	C_i^{*5}
Response	*R1*	*R2*	*R3*	*R4*	*R5*			DP			DPG	DPA
Weight [1]	*0.200*[b]	*0.200*	*0.200*	*0.200*	*0.200*							
Weight [2]	*0.259*	*0.148*	*0.333*	*0.111*	*0.148*							
Weight [3]	*0.167*	*0.233*	*0.200*	*0.133*	*0.267*							
1	**53.38**[b]	−1.94	−33.04	6.26	−39.80	**0.143**[c]	**0.075**[d]	**0.345**[e]	0.378	0.309	0.922	0.373
2	39.81	−4.47	−32.12	3.76	−39.62	0.160	0.048	**0.231**	0.252	0.228	0.606	0.744
3	54.90	3.91	−25.67	5.58	−37.24	0.118	0.094	**0.443**	0.489	0.424	0.774	0.317
4	60.02	16.57	−31.24	5.08	−38.91	0.068	0.141	**0.676**	0.684	0.673	0.664	0.320
5	64.40	24.98	−27.11	4.28	−40.00	0.041	0.176	**0.811**	0.837	0.831	0.425	0.289
6	58.11	10.39	−25.46	4.70	−39.56	0.093	0.117	**0.557**	0.597	0.550	0.404	0.529
7	24.22	−14.85	−32.88	5.31	−38.87	0.204	0.023	**0.101**	0.073	0.062	0.035	0.816
8	37.20	−0.54	−29.11	4.57	−34.32	0.142	0.065	**0.314**	0.320	0.313	0.452	0.494
9	49.68	31.77	−30.48	3.64	−33.64	0.042	0.199	**0.825**[f]	0.803	0.881	0.620	0.738
	151.70[a]	***47.70***	***89.44***	***14.60***	***114.19***							
Weighted Normalized Decision Matrix												
	v_{i1}	v_{i2}	v_{i3}	v_{i4}	v_{i5}							
1	**0.070**[b]	−0.008	−0.074	0.086	−0.070							
2	0.052	−0.019	−0.072	0.052	−0.069							
3	0.072	0.016	−0.057	0.076	−0.065							
4	0.079	0.069	−0.070	0.070	−0.068							
5	0.085	0.105	−0.061	0.059	−0.070							
6	0.077	0.044	−0.057	0.064	−0.069							
7	0.032	−0.062	−0.074	0.073	−0.068							
8	0.049	−0.002	−0.065	0.063	−0.060							
9	0.065	0.133	−0.068	0.050	−0.059							
	A = 0.085*	*0.133*	*−0.057*	*0.086*	*−0.059*							
	A- = 0.032	*−0.062*	*−0.074*	*0.050*	*−0.070*							

[a] The square root of sum of squares of each element in the columns.
[b] From Ref. [56]: 0.020*[(53.386)/(151.70)] = **0.070**.
[c] From Ref. [56]: $\{[(0.070)–(0.085)]^2 + \ldots \ldots + [(-0.059)-(-0.059)]^2\}^{1/2}$ = **0.143**.
[d] From Ref. [56]: $\{[(0.070)–(0.032)]^2 \ldots \ldots \ldots + [(-0.059)-(-0.070)]^2\}^{1/2}$ = **0.075**.
[e] From Ref. [56]: 0.143/(0.143 + 0.075) = **0.345**.
[f] Underlined values has been designated as optimum design.

Table 5
Improvement ratios.

Res.	Definition	Reference PVA1	Optimum DP (DP5)	Optimum DP (DP9)<	Optimum DPG (DPG9)	Optimum DPA (DPA7)
1	Hardness (MPa)	455.074	304.807	1658.932	450.131	994.514
2	Elastic modulus (GPa)	2.89	38.759	17.735	2.184	4.457
3	Contact angle (°)	51.38	33.41	22.68	43.43	36.09
4	Cp (J/g*°C)	1.951	1.521	1.637	1.869	1.795
5	Loss of weight (%)	57.18	48.08	99.98	98.66	92.13
Res.	Definition	Reference PVA2	Improvement or deterioration ratio for DP5	Improvement or deterioration ratio for DP9	Improvement or deterioration ratio for DPG9	Improvement or deterioration ratio for DPA7
1	Hardness (MPa)	807.308	−33.02[a]	105.49	−44.24	23.19
2	Elastic modulus (GPa)	2.392	1241.14[b]	641.43	−8.70	86.33
3	Contact angle (°)	49.07	34.97	53.78	11.49	26.45
4	Cp (J/g*°C)	2.13	−22.04	−23.15	−12.25	−15.73
5	Loss of weight (%)	97.06	15.91	−3.01	−1.65	5.08

[a] $\left[\left(\frac{304.807 - 455.074}{455.074}\right)*100\right] = -33.02$
[b] $\left[\left(\frac{38.759 - 2.89}{2.89}\right)*100\right] = 1241.14$

an 86.8 μm thickness, had 50.08 and 35.65 times higher elastic modulus (38.76 GPa) than the PVA/GO, with an 83.0 μm thickness, and the PVA/Ag, with a 90.0 μm thickness, respectively. The DOTP-added composites were successful in all other criteria, such as mechanical, hydrophilic and thermal performance, but not in specific heat value (Fig. 9).

5. Conclusions

In this study; for the first time, DOTP-added PVA composite films were produced, characterized and the quality characteristics of their properties were optimized. The DOTP-PVA composites were also modified with nanomaterials, such as GO and AgNPs, and these were

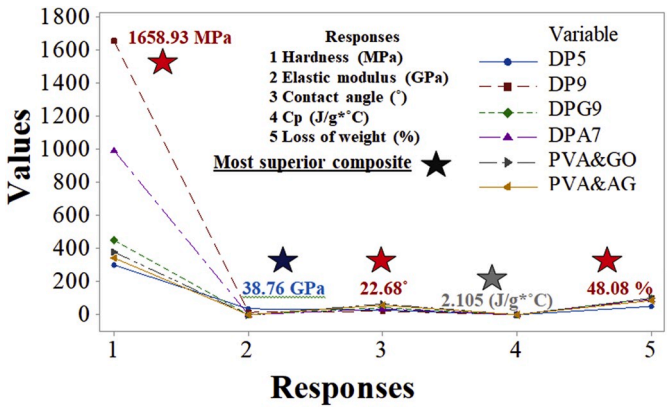

Fig. 9. Comparison with the widely used composite films.

compared with widely used PVA/GO and PVA/AgNPs composite films. The DP composite films and DP composite films modified with nanomaterials were characterized using FTIR and Raman spectroscopy.

DOTP, as organic filler, increased the hardness, elastic modulus and thermal stability of the PVA films, whilst the contact angle was reduced. By combining the TOPSIS and Taguchi methods in this study, DP composite films and DP composite films modified with nanomaterials were investigated through a multidimensional perspective and an application-based optimization methodology. By using TOPSIS-based Taguchi optimization, simultaneous improvements in the hardness (105.49%), elastic modulus (641.43%) and contact angle (53.78%) were achieved for DP9. On the other hand, this caused a lower weight loss, which can be improved by 15.91% by increasing the DOTP content for applications such as swabs, hydrophilic membranes and protecting packaging materials. DOTP with orthophthalate-free and non-carcinogenic properties must be used in these sectors. Thus, the solid waste disposal of PET can be provided effectively.

A small amount of GO (using 1% w/w instead of PVA) improved the composite films' properties, including their energy storage capabilities. However, GO above 1% by mass of PVA produced a more porous structure, with a possible tendency to agglomeration, thus losing its positive effect on the composite films and showing a tendency to worsen their properties. Smaller AgNPs led to greater hardness, elastic modulus and a lower contact angle. The results show that the modification of smaller AgNPs with PVA is effective, in terms of both mechanical and hydrophilic properties.

When the results of the study are evaluated, especially the textile and construction sectors seem more attractive for synthesized films. Synthesized films have a great potential to be used as, production of disposable underpad, industrial swabs and texturized yarns in the textile industry and synthetic fiber as reinforcement material in the construction industry because of its a high modulus of elasticity, hardness, hydrophilicity and thermal stability properties.

Declaration of competing interest

The authors declare that they have no conflict of interest.

Acknowledgements

This research was carried out with the support of the Scientific Research Project (MF061218D04) funded by Çankırı Karatekin University. Authors thank to Çankırı Karatekin University, Scientific Research Project Management Unit (ÇAKÜ-BAP).

Appendix A. Supplementary data

Supplementary data to this article can be found online at https://doi.org/10.1016/j.polymertesting.2019.106315.

References

[1] Y. Aryan, P. Yadav, S.R. Samadder, Life Cycle Assessment of the existing and proposed plastic waste management options in India: a case study, J. Clean. Prod. 211 (2019) 1268–1283.
[2] S.-A. Strungaru, R. Jijie, M. Nicoara, G. Plavan, C. Faggio, Micro- (nano) plastics in freshwater ecosystems: abundance, toxicological impact and quantification methodology, Trac. Trends Anal. Chem. 110 (2019) 116–128.
[3] L.S. Diaz-Silvarrey, A. McMahon, A.N. Phan, Benzoic acid recovery via waste poly (ethylene terephthalate) (PET) catalytic pyrolysis using sulphated zirconia catalyst, J. Anal. Appl. Pyrolysis 134 (2018) 621–631.
[4] M.N. Siddiqui, H.H. Redhwi, D.S. Achilias, Recycling of poly (ethylene terephthalate) waste through methanolic pyrolysis in a microwave reactor, J. Anal. Appl. Pyrolysis 98 (2012) 214–220.
[5] A. Carniel, É. Valoni, J.N. Junior, A. da Conceição Gomes, A.M. de Castro, Lipase from Candida Antarctica (CALB) and cutinase from Humicola insolens act synergistically for PET hydrolysis to terephthalic acid, Process Biochem. 59 (2017) 84–90.
[6] L.N.T. Ho, D.M. Ngo, J. Cho, H.M. Jung, Enhanced catalytic glycolysis conditions for chemical recycling of glycol-modified poly (ethylene terephthalate), Polym. Degrad. Stab. 155 (2018) 15–21.
[7] A.M. de Castro, A. Carniel, A novel process for poly (ethylene terephthalate) depolymerization via enzyme-catalyzed glycolysis, Biochem. Eng. J. 124 (2017) 64–68.
[8] M. Viante, T. Zanela, A. Stoski, E. Muniz, C. Almeida, Magnetic microspheres composite from poly (ethylene terephthalate)(PET) waste: synthesis and characterization, J. Clean. Prod. 198 (2018) 979–986.
[9] C. Liu, C. Shi, S. Zhu, R. Wei, C.-C. Yin, Structural and functional characterization of polyethylene terephthalate hydrolase from Ideonella sakaiensis, Biochem. Biophys. Res. Commun. 508 (2019) 289–294.
[10] J. Ding, J. Chen, Y. Ji, P. Ni, Z. Li, L. Xing, Kinetics of alcoholysis of poly(ethylene terephthalate) in sub- and super-critical isooctyl alcohol to produce dioctyl terephthalate, J. Anal. Appl. Pyrolysis 106 (2014) 99–103.
[11] K.E. García, R. Navarro, A. Ramírez-Hernández, Á. Marcos-Fernández, New routes to difunctional macroglycols using ethylene carbonate: reaction with bis-(2-hydroxyethyl) terephthalate and degradation of poly (ethylene terephthalate), Polym. Degrad. Stab. 144 (2017) 195–206.
[12] R.V. Moharir, S. Kumar, Challenges associated with plastic waste disposal and allied microbial routes for its effective degradation: a comprehensive review, J. Clean. Prod. 208 (2019) 65–76.
[13] J. Ding, J. Chen, Y. Ji, P. Ni, Z. Li, L. Xing, Kinetics of alcoholysis of poly (ethylene terephthalate) in sub-and super-critical isooctyl alcohol to produce dioctyl terephthalate, J. Anal. Appl. Pyrolysis 106 (2014) 99–103.
[14] B. Şimşek, T. Uygunoğlu, H. Korucu, M. Kocakerim, Performance of Dioctyl Terephthalate Concrete, Use of Recycled Plastics in Eco-Efficient Concrete, Elsevier, 2019, pp. 249–267.
[15] G. Xi, M. Lu, C. Sun, Study on depolymerization of waste polyethylene terephthalate into monomer of bis (2-hydroxyethyl terephthalate), Polym. Degrad. Stab. 87 (2005) 117–120.
[16] R. López-Fonseca, I. Duque-Ingunza, B. De Rivas, S. Arnaiz, J. Gutiérrez-Ortiz, Chemical recycling of post-consumer PET wastes by glycolysis in the presence of metal salts, Polym. Degrad. Stab. 95 (2010) 1022–1028.
[17] J. Purohit, G. Chawada, B. Choubisa, M. Patel, B. Dholakiya, Polyester polyol derived from waste poly (ethylene terephthalate) for coating application on mild steel, Chem. Sci. J. 2012 (CSJ-76) (2012) 1–7.
[18] A. Al-Sabagh, F. Yehia, A. Eissa, M. Moustafa, G. Eshaq, A. Rabie, A. ElMetwally, Cu-and Zn-acetate-containing ionic liquids as catalysts for the glycolysis of poly (ethylene terephthalate), Polym. Degrad. Stab. 110 (2014) 364–377.
[19] V. Jamdar, M. Kathalewar, K.A. Dubey, A. Sabnis, Recycling of PET wastes using electron beam radiations and preparation of polyurethane coatings using recycled material, Prog. Org. Coat. 107 (2017) 54–63.
[20] G. Malarvannan, M. Onghena, S. Verstraete, E. van Puffelen, A. Jacobs, I. Vanhorebeek, S.C.A.T. Verbruggen, K.F.M. Joosten, G. Van den Berghe, P. G. Jorens, A. Covaci, Phthalate and alternative plasticizers in indwelling medical devices in pediatric intensive care units, J. Hazard Mater. 363 (2019) 64–72.
[21] BASF starts up DOTP plasticizer and 2-EH feedstock plants at Pasadena site; reports 12% sales growth, Addit. Polym. 2017 (2017) 1–5.
[22] Oxea, Oxea aims to become major European supplier of DOTP plasticizer, Addit. Polym. 2018 (2018) 7.
[23] BASF to Produce DOTP Plasticizer in North America, Additives for Polymers, vol. 6, 2016, 2016.
[24] J. Chen, J. Lv, Y. Ji, J. Ding, X. Yang, M. Zou, L. Xing, Alcoholysis of PET to produce dioctyl terephthalate by isooctyl alcohol with ionic liquid as cosolvent, Polym. Degrad. Stab. 107 (2014) 178–183.
[25] O. Torpanyacharn, P. Sukpuang, A. Petchsuk, P. Opaprakasit, M. Opaprakasit, Curable precursors derived from chemical recycling of poly(ethylene terephthalate) and polylactic acid and physical properties of their thermosetting (co)polyesters, Polym. Bull. 75 (2018) 395–414.
[26] L. Nguyet Thi Ho, D. Minh Ngo, J. Cho, H.M. Jung, Enhanced catalytic glycolysis conditions for chemical recycling of glycol-modified poly(ethylene terephthalate), Polym. Degrad. Stab. 155 (2018) 15–21.
[27] L. Zhou, X. Lu, Z. Ju, B. Liu, H. Yao, J. Xu, Q. Zhou, Y. Hu, S. Zhang, Alcoholysis of polyethylene terephthalate to produce dioctyl terephthalate using choline chloride-

based deep eutectic solvents as efficient catalysts, Green Chem. 21 (2019) 897–906.
[28] B. Şimşek, T. Uygunoğlu, H. Korucu, M.M. Kocakerim, Analysis of the effects of dioctyl terephthalate obtained from polyethylene terephthalate wastes on concrete mortar: a response surface methodology based desirability function approach application, J. Clean. Prod. 170 (2018) 437–445.
[29] M.M. Vopson, J. Naylor, T. Saengow, E.G. Rogers, S. Lepadatu, Y.K. Fetisov, Development of flexible Ni80Fe20 magnetic nano-thin films, Phys. B Condens. Matter 525 (2017) 12–15.
[30] A. Voronov, S. Atarah, Control and broadband monitoring of transparent multilayer thin films deposited by magnetron sputtering, Surf. Coat. Technol. 347 (2018) 252–256.
[31] M. Rao, M. Shekhawat, A brief survey on basic properties of thin films for device application, in: International Journal of Modern Physics: Conference Series, World Scientific, 2013, pp. 576–582.
[32] R. Smith, C. Crespo, M. Aboy, Review of recent patents on flexible photovoltaic applications in portable and niche markets, Recent Pat. Eng. 7 (2013) 153–166.
[33] P.S. Brown, B. Bhushan, Mechanically durable, superoleophobic coatings prepared by layer-by-layer technique for anti-smudge and oil-water separation, Sci. Rep. 5 (2015) 8701.
[34] A. Eshaghi, A.A. Aghaei, Transparent hydrophobic micro-nano silica-silica nano-composite thin film with environmental durability, Mater. Chem. Phys. 227 (2019) 318–323.
[35] Q. Wu, Y. Lv, L. Lin, X. Zhang, Y. Liu, X. Zhou, An improved thin-film electrode for vanadium redox flow batteries enabled by a dual layered structure, J. Power Sources 410–411 (2019) 152–161.
[36] M. Yu, X. Feng, Thin-Film Electrode-Based Supercapacitors, Joule, 2019.
[37] A.H. Elsheikh, S.W. Sharshir, M.K. Ahmed Ali, J. Shaibo, E.M.A. Edreis, T. Abdelhamid, C. Du, Z. Haiou, Thin film technology for solar steam generation: a new dawn, Sol. Energy 177 (2019) 561–575.
[38] M. Salah, P. Murphy, C. Hall, C. Francis, R. Kerr, M. Fabretto, Pure silicon thin-film anodes for lithium-ion batteries: a review, J. Power Sources 414 (2019) 48–67.
[39] A. Timoumi, S.N. Alamri, H. Alamri, The development of TiO2-graphene oxide nano composite thin films for solar cells, Res. Phys. 11 (2018) 46–51.
[40] M. Ghahremani Honarvar, M. Latifi, Overview of wearable electronics and smart textiles, J. Text. Inst. 108 (2017) 631–652.
[41] K. Li, S. Jin, H. Chen, J. Li, Bioinspired interface engineering of gelatin/cellulose nanofibrils nanocomposites with high mechanical performance and antibacterial properties for active packaging, Compos. B Eng. 171 (2019) 222–234.
[42] B.C. Sertel, N.A. Sonmez, M.D. Kaya, S. Ozcelik, Development of MgO:TiO2 thin films for gas sensor applications, Ceram. Int. 45 (2019) 2917–2921.
[43] K.E. Bourakadi, N. Merghoub, M. Fardioui, M.E.M. Mekhzoum, I.M. Kadmiri, E. M. Essassi, A.E.K. Qaiss, R. Bouhfid, Chitosan/polyvinyl Alcohol/thiabendazoluim-Montmorillonite Bio-Nanocomposite Films: Mechanical, Morphological and Antimicrobial Properties, Composites Part B: Engineering, 2019.
[44] A. Ali, M.A. Shahid, Polyvinyl alcohol (PVA)–Azadirachta indica (neem) nanofibrous mat for biomedical application: formation and characterization, J. Polym. Environ. 27 (2019) 2933–2942.
[45] S. Hakim, M.R.R. Darounkola, HaniehTalari, M. Barghemadi, M. Parvazinia, Fabrication of PVA/nanoclay hydrogel nanocomposites and their microstructural effect on the release behavior of a potassium phosphate fertilizer, J. Polym. Environ. 27 (2019) 2925–2932.
[46] D. Yin, A. Xiang, Y. Li, H. Qi, H. Tian, G. Fan, Effect of plasticizer on the morphology and foaming properties of poly(vinyl alcohol) foams by supercritical CO2 foaming agents, J. Polym. Environ. 27 (2019) 2878–2885.
[47] M.B. Tahir, A.M. Asiri, G. Nabi, M. Rafique, M. Sagir, Fabrication of heterogeneous photocatalysts for insight role of carbon nanofibre in hierarchical WO3/MoSe2 composite for enhanced photocatalytic hydrogen generation, Ceram. Int. 45 (2019) 5547–5552.
[48] M.B. Tahir, M. Sagir, M. Zubair, M. Rafique, I. Abbas, M. Shakil, I. Khan, S. Afsheen, A. Hasan, A. Ahmed, WO3 nanostructures-based photocatalyst approach towards degradation of RhB dye, J. Inorg. Organomet. Polym. Mater. 28 (2018) 1107–1113.
[49] N.R. Khalid, M. Liaqat, M.B. Tahir, G. Nabi, T. Iqbal, N.A. Niaz, The role of graphene and europium on TiO2 performance for photocatalytic hydrogen evolution, Ceram. Int. 44 (2018) 546–549.
[50] S. Gahlot, V. Kulshrestha, G. Agarwal, P.K. Jha, Synthesis and Characterization of PVA/GO Nanocomposite Films, Macromolecular Symposia, Wiley Online Library, 2015, pp. 173–177.
[51] S. Kashyap, S.K. Pratihar, S.K. Behera, Strong and ductile graphene oxide reinforced PVA nanocomposites, J. Alloy. Comp. 684 (2016) 254–260.
[52] M. Goumri, C. Poilâne, P. Ruterana, B.B. Doudou, J. Wéry, A. Bakour, M. Baitoul, Synthesis and characterization of nanocomposites films with graphene oxide and reduced graphene oxide nanosheets, Chin. J. Phys. 55 (2017) 412–422.
[53] V. Hebbar, R. Bhajantri, H. Ravikumar, S. Ningaraju, Role of free volumes in conducting properties of GO and rGO filled PVA-PEDOT: PSS composite free standing films: a positron annihilation lifetime study, J. Phys. Chem. Solids 126 (2019) 242–256.
[54] M.B. Tahir, G. Nabi, N.R. Khalid, Enhanced photocatalytic performance of visible-light active graphene-WO3 nanostructures for hydrogen production, Mater. Sci. Semicond. Process. 84 (2018) 36–41.
[55] K. Shahzad, M.B. Tahir, M. Sagir, Engineering the performance of heterogeneous WO3/fullerene@Ni3B/Ni(OH)2 photocatalysts for hydrogen generation, Int. J. Hydrogen Energy 44 (2019) 21738–21745.
[56] R.P. Chahal, S. Mahendia, A. Tomar, S. Kumar, SHI irradiated PVA/Ag nanocomposites and possibility of UV blocking, Opt. Mater. 52 (2016) 237–241.
[57] H. Koduru, L. Marino, V. Janardhanam, N. Scaramuzza, Influence of thin layer of silver nanoparticles on optical and dielectric properties of poly (vinyl alcohol) composite films, Surf. Interfaces 5 (2016) 47–54.
[58] P. Mukherjee, A. Das, B. Dutta, A. Meikap, Role of silver nanotube on conductivity, dielectric permittivity and current voltage characteristics of polyvinyl alcohol-silver nanocomposite film, J. Phys. Chem. Solids 111 (2017) 266–273.
[59] A. El-Shamy, A. Maati, W. Attia, K.A. El-Kader, Promising method for preparation the PVA/Ag nanocomposite and Ag nano-rods, J. Alloy. Comp. 744 (2018) 701–711.
[60] H. Korucu, B. Şimşek, A. Yartaşı, A TOPSIS-based Taguchi design to investigate optimum mixture proportions of graphene oxide powder synthesized by Hummers method, Arabian J. Sci. Eng. 43 (2018) 6033–6055.
[61] B. Şimşek, G. Ultav, H. Korucu, A. Yartaşı, Improvement of the graphene oxide dispersion properties with the use of TOPSIS based Taguchi application, Period. Polytech. - Chem. Eng. 62 (3) (2018) 323–335.
[62] Ö. Karhan, Ö.B. Ceran, O.N. Şara, B. Şimşek, Response surface methodology based desirability function approach to investigate optimal mixture ratio of silver nanoparticles synthesis process, Ind. Eng. Chem. Res. 56 (2017) 8180–8189.
[63] E. Ondari Nyakundi, M.N. Padmanabhan, Green chemistry focus on optimization of silver nanoparticles using response surface methodology (RSM) and mosquitocidal activity: Anopheles stephensi (Diptera: Culicidae), Spectrochim. Acta A Mol. Biomol. Spectrosc. 149 (2015) 978–984.
[64] B. Şimşek, Y.T. İç, E.H. Şimşek, A TOPSIS-based Taguchi optimization to determine optimal mixture proportions of the high strength self-compacting concrete, Chemometr. Intell. Lab. Syst. 125 (2013) 18–32.
[65] B. Şimşek, T. Uygunoğlu, Multi-response optimization of polymer blended concrete: a TOPSIS based Taguchi application, Constr. Build. Mater. 117 (2016) 251–262.
[66] B. Şimşek, TOPSIS based Taguchi design optimization for CVD growth of graphene using different carbon sources: graphene thickness, defectiveness and homogeneity, Chin. J. Chem. Eng. 27 (3) (2019) 685–694.
[67] A.L.M. Vargas, E. Blando, R. Hübler, Elasto – plastic materials behavior evaluation according to different models applied in indentation hardness tests, Measurement 139 (2019) 134–139.
[68] S.K. Thimmappa, B.R. Golla, V.V. Bhanu Prasad, B. Majumdar, B. Basu, Phase stability, hardness and oxidation behaviour of spark plasma sintered ZrB2-SiC-Si3N4 composites, Ceram. Int. 45 (2019) 9061–9073.
[69] T. Xie, J. Zhu, L. Fu, R. Zhang, N. Li, M. Yang, J. Wang, W. Qin, W. Yang, D. Li, L. Zhou, The evolution of hardness in Cu-W alloy thin films, Mater. Sci. Eng. A 729 (2018) 170–177.
[70] N.A. Sakharova, M.C. Oliveira, J.M. Antunes, J.V. Fernandes, On the determination of the film hardness in hard film/substrate composites using depth-sensing indentation, Ceram. Int. 39 (2013) 6251–6263.
[71] R. Aghaei, A. Eshaghi, A.A. Aghaei, Durable transparent super-hydrophilic hollow SiO2-SiO2 nanocomposite thin film, Mater. Chem. Phys. 219 (2018) 347–360.
[72] F. Tang, Q.-W. Yu, B.-F. Yuan, Y.-Q. Feng, Hydrophilic materials in sample pretreatment, Trac. Trends Anal. Chem. 86 (2017) 172–184.
[73] L. Rivière, N. Caussé, A. Lonjon, É. Dantras, C. Lacabanne, Specific heat capacity and thermal conductivity of PEEK/Ag nanoparticles composites determined by Modulated-Temperature Differential Scanning Calorimetry, Polym. Degrad. Stab. 127 (2016) 98–104.
[74] K. Chen, J. Liu, X. Yang, D. Zhang, Preparation, optimization and property of PVA-HA/PAA composite hydrogel, Mater. Sci. Eng. C 78 (2017) 520–529.
[75] F. Liu, J. Chen, Z. Li, P. Ni, Y. Ji, Q. Meng, Alcoholysis of poly(ethylene terephthalate) to produce dioctyl terephthalate with sub- and super-critical isooctyl alcohol, J. Anal. Appl. Pyrolysis 99 (2013) 16–22.
[76] G. Kandhol, H. Wadhwa, S. Chand, S. Mahendia, S. Kumar, Study of dielectric relaxation behavior of composites of Poly (vinyl alcohol) (PVA) and Reduced graphene oxide (RGO), Vacuum 160 (2019) 384–393.
[77] C.-H. Lai, G.-A. Wang, T.-K. Ling, T.-J. Wang, P.-k. Chiu, Y.-F. Chou Chau, C.-C. Huang, H.-P. Chiang, Near infrared surface-enhanced Raman scattering based on star-shaped gold/silver nanoparticles and hyperbolic metamaterial, Sci. Rep. 7 (2017) 5446.
[78] M.J. Yoo, H.B. Park, Effect of hydrogen peroxide on properties of graphene oxide in Hummers method, Carbon 141 (2019) 515–522.
[79] X. Zhou, C. Wang, C. Fang, R. Yu, Y. Li, W. Lei, Structure and thermal properties of various alcoholysis products from waste poly(ethylene terephthalate), Waste Manag. 85 (2019) 164–174.
[80] N. Yadav, B. Lochab, A comparative study of graphene oxide: Hummers, intermediate and improved method, FlatChem 13 (2019) 40–49.
[81] K. Jyoti, M. Baunthiyal, A. Singh, Characterization of silver nanoparticles synthesized using Urtica dioica Linn. leaves and their synergistic effects with antibiotics, J. Radiat. Res. Appl. Sci. 9 (2016) 217–227.
[82] A.C. Ferrari, J.C. Meyer, V. Scardaci, C. Casiraghi, M. Lazzeri, F. Mauri, S. Piscanec, D. Jiang, K.S. Novoselov, S. Roth, A.K. Geim, Raman spectrum of graphene and graphene layers, Phys. Rev. Lett. 97 (2006) 187401.
[83] J. Qin, M.S. Kim, K. Chao, S. Dhakal, B.-K. Cho, S. Lohumi, C. Mo, Y. Peng, M. Huang, Advances in Raman spectroscopy and imaging techniques for quality and safety inspection of horticultural products, Postharvest Biol. Technol. 149 (2019) 101–117.
[84] P. Tan, J. Wen, Y. Hu, X. Tan, Adsorption of Cu2+ and Cd2+ from aqueous solution by novel electrospun poly(vinyl alcohol)/graphene oxide nanofibers, RSC Adv. 6 (2016) 79641–79650.
[85] Y. Cai, X. Piao, W. Gao, Z. Zhang, E. Nie, Z. Sun, Large-scale and facile synthesis of silver nanoparticles via a microwave method for a conductive pen, RSC Adv. 7 (2017) 34041–34048.

[86] K.S. Novoselov, A.K. Geim, S.V. Morozov, D. Jiang, Y. Zhang, S.V. Dubonos, I. V. Grigorieva, A.A. Firsov, Electric field in atomically thin carbon films, Science 306 (2004) 666–669.
[87] J. Guerrero-Contreras, F. Caballero-Briones, Graphene oxide powders with different oxidation degree, prepared by synthesis variations of the Hummers method, Mater. Chem. Phys. 153 (2015) 209–220.
[88] C. Zhou, F. Li, J. Hu, M. Ren, J. Wei, Q. Yu, Enhanced mechanical properties of cement paste by hybrid graphene oxide/carbon nanotubes, Constr. Build. Mater. 134 (2017) 336–345.
[89] Q. Wang, D.-G. Yu, L.-L. Zhang, X.-K. Liu, Y.-C. Deng, M. Zhao, Electrospun hypromellose-based hydrophilic composites for rapid dissolution of poorly water-soluble drug, Carbohydr. Polym. 174 (2017) 617–625.
[90] S.B. Rekik, S. Gassara, J. Bouaziz, A. Deratani, S. Baklouti, Enhancing hydrophilicity and permeation flux of chitosan/kaolin composite membranes by using polyethylene glycol as porogen, Appl. Clay Sci. 168 (2019) 312–323.
[91] X. Qi, X. Yao, S. Deng, T. Zhou, Q. Fu, Water-induced shape memory effect of graphene oxide reinforced polyvinyl alcohol nanocomposites, J. Mater. Chem. 2 (2014) 2240–2249.